Engineering Structures 198 (2019) 109427

Contents lists available at ScienceDirect

Engineering Structures

journal homepage: www.elsevier.com/locate/engstruct

Fragility-based sensitivity analysis on the seismic performance of pile-group-supported bridges in liquefiable ground undergoing scour potentials

Xiaowei Wang[a,b], Aijun Ye[b], Bohai Ji[a,*]

[a] College of Civil and Transportation Engineering, Hohai University, Nanjing 210024, China
[b] State Key Lab of Disaster Reduction in Civil Engineering, Tongji University, Shanghai 200092, China

ARTICLE INFO

Keywords:
Bridge
Sensitivity
Seismic fragility
Scour
Liquefaction
Tornado diagram

ABSTRACT

Characterizing the effect of varying model parameters on the seismic performance of bridges is a desirable assistance to retrofits of existing bridges and designs of new bridges, especially for those in complex geotechnical conditions where scour and liquefaction potentials are involved. This paper aims to rank the sensitivity of fourteen structural and soil parameters for seismic performance assessment of pile-group-supported bridges in liquefiable ground undergoing scour potentials. To this end, a fragility-based Tornado diagram method for sensitivity analyses is proposed first in this study. An experimentally validated soil-foundation-bridge coupled finite element model considering scour and liquefaction effects is adopted and excited by a set of real ground motions for fragility analyses. Results indicate that the effect of scour depth slightly influence the most sensitive parameters, mainly including column height and diameter and pile diameter, for the performance of bridge components (i.e., bearing, column and pile). However, the increase of scour depth does downgrade the relative sensitivity of column-associated ones (e.g., column height and axial compressive ratio) and soil-related ones (i.e., loose and dense sand relative densities), while upgrade that of the pile-associated ones (e.g., pile diameter, center-to-center distance and longitudinal reinforcement ratio). In addition, to abide the capacity design principle that columns should fail before pile foundations, designs or retrofits of bridges using relatively larger pile diameter, column height, material strengths and longitudinal/transverse reinforcement ratios, together with smaller column diameter and pile center-to-center distance are recommended for mitigating scour and liquefaction effects on the seismic performance of pile foundations.

1. Introduction

Scour has been reported as one of the most severe hazards causing bridge failures [1,2]. Fig. 1 shows an example of typical multi-span bridges subjected to the scour hazard, in which pile foundations were exposed without confinements of surrounding soils, leading to the degradation of lateral capacity of the bridges. On the other hand, saturated soils, especially cohesionless ones, in scoured bridge sites probably liquefy under following earthquakes. Liquefaction-induced damage to pile foundations and associated bridge failures have been reported in many earthquake events [3,4]. Previous studies on the seismic behavior of bridges, regardless of field and laboratory experiments (e.g., [5–9]) or numerical analyses (e.g., [10–14]), often considered the effect of liquefaction or scour, separately. However, it tends to be common in practice that bridges are located in flood-induced scour sites where saturated sands may liquefy under earthquakes. In this regard, Wang et al. [15] recently reported the first shake-table test on scoured pile-group-supported bridges in liquefiable soils. Moreover, scour can affect wave propagations in soils [16], thereby affecting liquefaction potentials as well as the seismic behavior of bridges. Hence, predictions of the seismic performance of bridges in complex geotechnical conditions such as scour and liquefaction require special attentions.

Numerical predictions on the seismic performance of soil-bridge systems may be susceptible to varying model parameters. From a predictive point of view, it is desirable to characterize impacts of these parameters to assist in seismic retrofits and designs of bridges. For this purpose, previous studies have identified key parameters and their variations in response prediction and performance assessment of bridges in non-scoured and non-liquefiable ground [17–19] as well as in scour or liquefiable ground, separately [20–22]. To the best knowledge of the authors, critical parameters for seismic performance of bridges under combined effects of scour and liquefaction hazards have not been documented well. Furthermore, impacts of scour depths and structural

* Corresponding author.
E-mail addresses: x.wang@hhu.edu.cn (X. Wang), yeaijun@tongji.edu.cn (A. Ye), bhji@hhu.edu.cn (B. Ji).

https://doi.org/10.1016/j.engstruct.2019.109427
Received 9 March 2019; Received in revised form 19 July 2019; Accepted 20 July 2019
Available online 03 August 2019

Fig. 1. Scour-induced exposures of pile foundations for two parallel regular multi-span bridges (By courtesy of Professor Yi-Ching Lin).

damage limit states on sensitivity rankings of these parameters have never been reported. These gaps stimulate the motivation for the present study.

This study aims to identify structural and soil parameters that have the most and least sensitive effects on the seismic performance assessment of bridges in liquefiable ground that undergoes scour potentials. Attentions are also paid to the effects of scour depths and damage limit states on the relative sensitivity of the parameters. To this end, a fragility-based Tornado diagram approach for sensitivity analyses is proposed first. A coupled soil-pile-structure finite element (FE) model is validated by a centrifuge test in literature. Then, a coupled soil-foundation-bridge FE model, which represents typical pile-group-supported multi-span reinforced concrete (RC) bridges in liquefiable ground undergoing scour potentials, is excited by a set of real ground motions for fragility analyses. Finally, sensitivity results of the studied fourteen parameters are discussed to provide insights into designs and retrofits of bridges in liquefiable ground subjected to scour potentials. This study can provide a research basis for future optimization study on the seismic design of bridges in complex geotechnical conditions where significant soil-foundation-structure interactions are involved [23].

2. Methodology

There are several methods for sensitivity analyses in civil engineering, primarily including Tornado diagram, First-Order-Second-Moment and Monte Carlo simulation. Among them, the Monte Carlo simulation often requires heavy computational efforts, especially for nonlinear dynamic analyses that involve complex soil-foundation-structure interactions. The application range of First-Order-Second-Moment method falls into circumstances where demands exhibit a linear trend (or slightly nonlinear) across the varied parameters. Such circumstances are often difficult to meet for bridges in liquefiable soils, as high levels of nonlinearities are often involved. By contrast, Tornado diagram, which is adopted in this study, is an efficient solution from a view of practice. Moreover, this study concentrates on the seismic performance assessment (i.e., considering both the demand and capacity), rather than the seismic demand assessment merely. Hence, fragility analyses are used to rigorously estimate the seismic performance of bridges. In addition, fragility analyses can efficiently assess the performance at multiple damage limit states. Considering these merits, a fragility-based Tornado diagram method is proposed in this study for sensitivity analyses. Fig. 2 illustrates the process of this method described as below.

For a parameter supposing a normal or lognormal distribution, two extreme values at 16th and 84th percentiles (i.e. mean, μ, minus and plus standard deviation, σ) are adopted as lower and upper bounds, respectively. A set of real ground motions (described later) is selected for dynamic analyses of three FE models that adopt parameters with the lower, mean and upper values, respectively. Probabilistic seismic demand analyses using Cloud method [24] are performed to build the corresponding three probabilistic seismic demand models (PSDMs), which represent probabilistic relationships between engineering demand parameters (EDPs) and intensity measures (IMs). According to the mathematical basis of fragility curves [24] and the pre-defined probabilistic capacity models (described later), three fragility curves that reflect the impact of this parameter on the seismic performance are generated using Eq. (1).

$$P[D \geqslant C|IM] = 1 - \Phi\left(\frac{\ln(S_C) - \ln(S_D)}{\sqrt{\beta_C^2 + \beta_D^2}}\right) \quad (1)$$

where $\Phi(\bullet)$ is the standard normal cumulative distribution function, D is the demand, C is the capacity, S_D and S_C are median values of the demand and capacity, respectively, β_D and β_C are logarithmic standard deviations of the demand and capacity, respectively. Based on the fragility curves, IM values at a given level of probability of exceedance, P_r (e.g., 50%, the so-called median fragility values, as used in this study) are obtained as the "performance indices" (i.e., $IM_{\mu-\sigma}$, IM_{μ} and $IM_{\mu+\sigma}$, as shown in Fig. 2) for this parameter in Tornado diagram. Note that the blue (dark) bars in Tornado diagram represent $IM_{\mu+\sigma}$ while the orange (bright) ones refer to $IM_{\mu-\sigma}$. The bar in the right side of the Tornado diagram represents the case with a lower probability of exceedance, indicating an improved performance for that parameter. Repeating the above process for every studied parameter. The obtained performance indices are sorted from high to low based on their ranges, R_{IM}, as defined in Eq. (2), to fulfill the Tornado diagram.

$$R_{IM} = |IM_{\mu+\sigma} - IM_{\mu}| + |IM_{\mu} - IM_{\mu-\sigma}| \quad (2)$$

where $|\bullet|$ is the absolute value operator. It is worth noting that due to high levels of nonlinearities for cases with particular parameters, fragility curves derived from these models with the mean values (μ) may not lay between the upper ($\mu + \sigma$) and lower (μ-σ) counterparts (see "Param N" in Fig. 2, in which the blue (dark) bar is partially covered by the orange (bright) one). The adopted absolute value operator in Eq. (2) can consider the total distances between $IM_{\mu-\sigma}$ (or $IM_{\mu+\sigma}$) and IM_{μ} for such parameters.

3. Numerical modelling and validation

3.1. Description of centrifuge test

To validate the numerical modelling technique adopted in this study, a centrifuge test named CSP3 and performed by Wilson [25], which investigated the behavior of pile-supported structures in liquefied soils, is simulated. Fig. 3 shows the test setup, in which a 0.67 m-diameter/0.06 m-thickness steel-pipe pile with a lumped mass of 49 ton is embedded 16.76 m into saturated medium dense Nevada sand with a relative density, D_r = 55% overlying dense Nevada sand (D_r = 80%). Several sensors were installed to monitor the soil and structural responses under the 0.49g Santa Cruz ground motion, as depicted in Fig. 4.

3.2. Finite element modelling

To model the above described centrifuge test [25], a coupled multi-dimensional soil-pile-structure FE model is built in *OpenSees* [26]. Fig. 5 schematically illustrates the FE model. Two-dimensional plain-strain soil columns are linked to three-dimensional piles through one-dimensional soil-pile springs. The reason to adopt such a multi-dimensional modelling is for purposes of modelling expediencies and computational efficiencies in soil domains as well as accurately modelling spatial features of structures such as pile groups that are studied later in this paper. More specifically, pressure-dependent multi-yield (PDMY) materials are assigned to four-node QuadUP shear-beam elements to

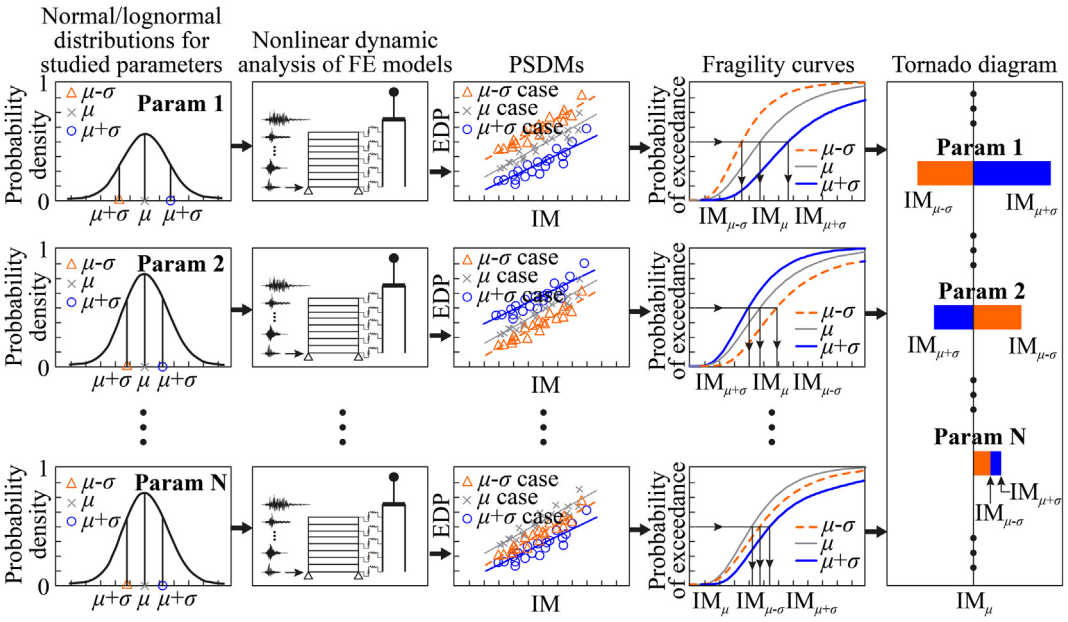

Fig. 2. Illustration of the fragility-based Tornado diagram for sensitivity analysis.

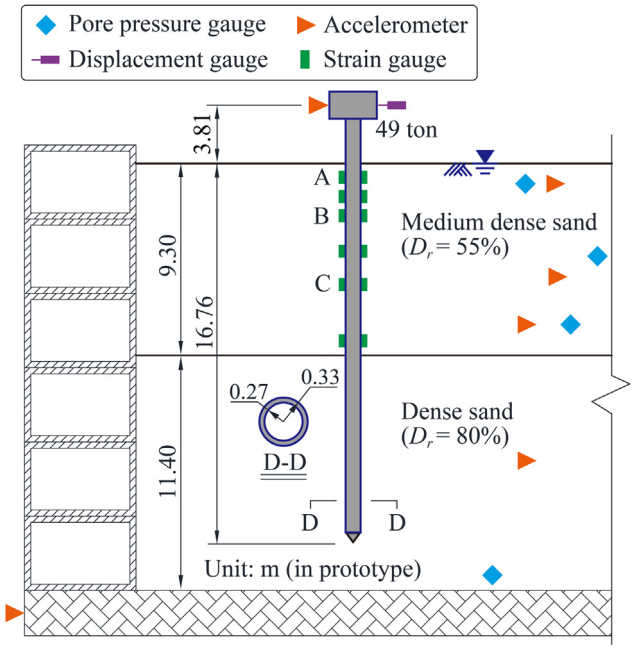

Fig. 3. Test setup of Centrifuge Test CSP3 (Replotted from [25]).

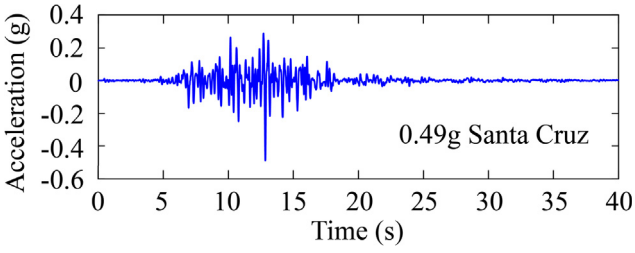

Fig. 4. Santa Cruz motion at the shear box base of Centrifuge Test CSP3 (Data from [25]).

simulate liquefaction under cyclic excitations [27]. This simplified two-dimensional modeling technique for soil column has been verified by many studies (e.g., [11,28]). Table 1 lists parameters for constitutive models of the Nevada sands used in the centrifuge test. Soil-pile springs are modeled using the PyLiq1 and TzLiq1 materials for the lateral resistance (*p-y* spring) and vertical friction (*t-z* spring), respectively, and the QzSimple1 material for the vertical resistance at pile tip (*q-z* spring) [29]. These soil springs have been widely adopted in many studies involving liquefiable soil-pile interactions (e.g., [28,30], among others). Soil liquefaction can be represented by the excess pore pressure ratio, $r_u = \Delta u/\sigma'_{v0}$, where Δu is the recorded variation of pore pressure at a depth, and σ'_{v0} is the initial effective overburden stress at that depth. Effects of excess pore pressure ratios or variations in soil effective stresses are considered by changing the constitutive models of soil-pile springs during liquefaction [29]. Piles and structures can be modeled using elastic or nonlinear beam-column elements depending on the behavior of the piles and structures under earthquakes. For the studied centrifuge test, elastic beam-column elements are adopted, as the pile practically behaved is the elastic state.

3.3. Model validation: Numerical predictions versus test records

The numerical model is validated by comparisons between recorded and predicted results in terms of pore pressure ratio developments (Fig. 6), soil acceleration responses (Fig. 7), superstructure acceleration and displacement responses (Fig. 8), and pile bending moment responses (Fig. 9). Qualitatively, good agreements are observed from these figures. Quantitatively, errors of the peak responses are generally within 20% (most of them are within 10%). These results validate the numerical modelling technique, which is capable of predicting seismic responses of soils and piles accounting for liquefaction effects.

4. Studied soil-bridge system, parameters and ground motions

4.1. Scope of studied soil-bridge system and FE modelling

The scope of the studied soil-bridge system falls into regular multi-span RC girder bridges with multiple bents, each supported by a pile-group foundation subjected to scour and liquefaction potentials. For conciseness and simplification, this study focuses on the transverse direction. In this direction, the bridges are supposed to have a fairly uniform distribution of stiffness and strength among the bents, i.e., almost identical structural configurations, soil profiles and scour depths among the bents, such as the practice case shown in Fig. 1. For this

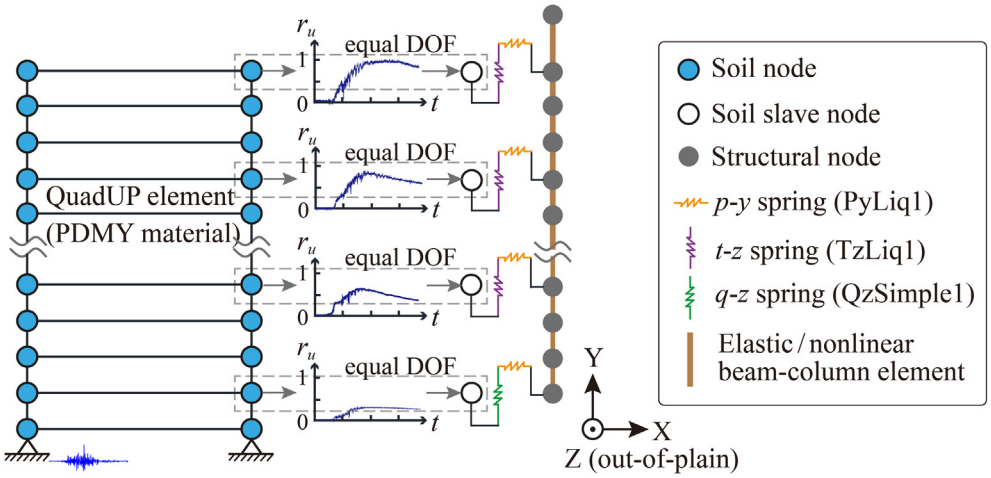

Fig. 5. Schematic of multi-dimensional modelling for liquefiable soil-structure interaction.

Table 1
Parameters for constitutive models (PDMY) of Nevada sand used in the centrifuge test.

Parameter (Unit)	Upper layer	Lower layer	Description and source [Reference]
*D_r (%)	55	80	Relative density measured in the test
*$(N_1)_{60}$	18.2	38.4	Standard penetration test blow counts, $(N_1)_{60}= 60D_r^2$ [31]
*G_s	2.65	2.65	Empirical specific density of Nevada sand [25]
*e_{min}	0.516	0.516	Empirical minimum void ratio of Nevada sand [32]
*e_{max}	0.894	0.894	Empirical maximum void ratio of Nevada sand [32]
e	0.686	0.592	Void ratio, $e = e_{max}-D_r(e_{max}-e_{min})$ [33]
ρ (ton/m^3)	1.98	2.04	Saturated density, $\rho= \rho_w(G_s+e)/(1+e)$, ρ_w=1.0 [33]
φ	33	37	Friction angle of sand, related to D_r [34]
$f_r^{'}$(kPa)	80	80	Reference pressure [27,35]
*V_s (m/s)	181	215	Shear wave velocity, $V_s=85((N_1)_{60}+2.5)^{0.25}$ [36]
*G_{max} (MPa)	65.0	94.1	Maximum shear modulus, $G_{max}= \rho V_s^2$ [37]
$G_{max,oct}$ (MPa)	79.6	115	Octahedral shear modulus, $G_{max,oct} = \sqrt{1.5}G_{max}$ [27,35]
γ_{max}	0.1	0.1	Maximum shear strain [27,35]
*θ	0.33	0.33	Empirical Poison's ratio [32]
*B/G	2.67	2.67	Bulk/shear modulus ratio $B/G = 2(1+\hat{1}_v)/[3(1-2\hat{1}_v)]$ [27,35]
B_r (MPa)	212	307	Bulk modulus, $B_r = (B/G)G_{max,oct}$ [27,35]
d_p	0.5	0.5	Pressure dependent factor, 0 means independent [27,35]
c	0.0278	0.0188	Coefficient defines the rate of volume decrease (i.e., contraction), $c = -0.024\ln(100D_r)+0.124$ [38]
d_1	0.4	0.6	Coefficients define the rate of volume increase (i.e., dilation); larger values correspond to stronger rate [27,35]
d_2	2	3	
Liq_1	10	5	Liq_1 defines the effective confining pressure below which is in effect. Liq_2 and Liq_3 control the plastic shear strain accumulation,
Liq_2	0.1	0.003	i.e. cyclic mobility [27,35]
Liq_3	1	1	

* Not input parameters for constitutive models, but for determining the constitutive parameters.

reason, abutments are not considered in the present study. In this regard, the transverse responses of the studied bridges can be represented by a single bent. Such a simplified modelling strategy has been used in several former studies [39–42].

Fig. 10 schematically shows the multi-dimensional modelling of the studied soil-bridge system in *OpenSees* [26]. A 3 × 2 pile-group-supported single column with a lumped mass is embedded into a two-layered soil profile. The soil column is meshed into 0.5 m-thickness. Before scour, an 8 m-thickness loose sand layer overlies a 22 m-thickness dense sand layer. Parts of the upper loose sand layer, depths of 3 m and 6 m, are removed to represent two general scour scenarios, which together with the scenario before scour form the three scour scenarios considered in this study (i.e., no scour, scour 3 m, and scour 6 m). These scour depths fall into the common range of general scour depth in practice [43]. As for the three-dimensional modelling of structures, piles and the single column are modeled using displacement-based beam-column elements, each with a length of 0.5 m and five integration points. The concrete fiber model is represented by the *Concrete04* material [44], as depicted in Fig. 10(b), where the strain at the compressive strength of concrete cover, $\varepsilon_{c,cover}$ = 0.002 and the ultimate strain of the concrete cover, $\varepsilon_{cu,cover}$ = 0.005, while parameters of the concrete core are determined based on Mander et al. [44]. The steel fiber model is represented by the *Steel02* material [45], as shown in Fig. 10(c), in which the hardening ratio, b = 0.01, while other parameters are described later in this paper. The RC cap is modeled using elastic beam-column elements with large stiffness. The lumped mass, M_{ss}, that represents the deck is set as $M_{ss} = R_{ac}{\cdot}f_c{\cdot}A_g/g$, where R_{ac} is the axial compressive ratio, f_c is the compressive strength of the concrete cover, A_g is the gross section of the column and g is the gravity constant. Values of these parameters (described later) represent common practices [46]. Elastic rubber bearings (ERBs) are used to connect the single column to the lumped mass. The constitutive model refers to Zhang and Huo [47], as illustrated in Fig. 10(d), in which the shear modulus of the rubber, G_b = 1200 kN/m, the total thickness of the rubber layers, t_r = 0.07 m, and the total area of the bearing, A_b is determined according to AASHTO [48]. The ERB model is assigned to the transverse degree-of-freedom while other degree-of-freedoms are fixed to represent configurations in the transverse direction. Following the

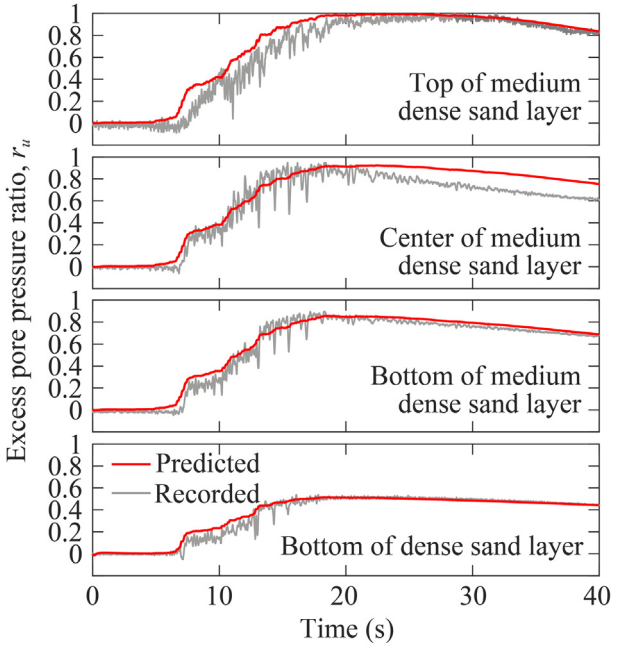

Fig. 6. Model validation: Developments of excess pore pressure ratios.

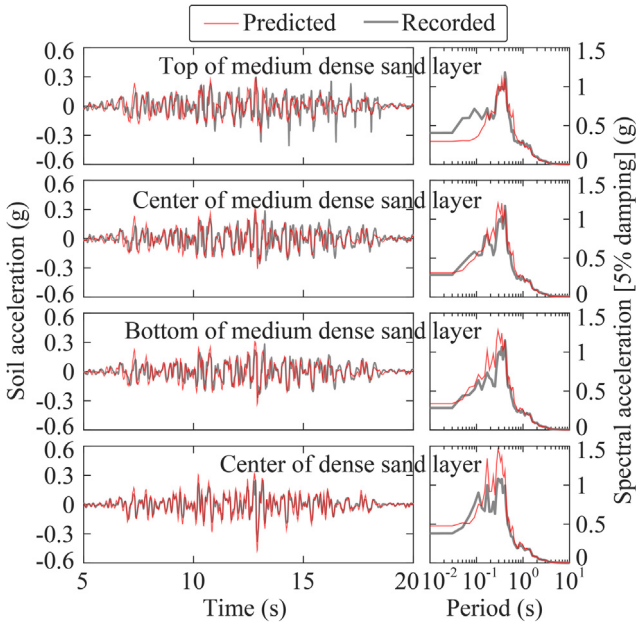

Fig. 7. Model validation: Time histories of soil accelerations and associated spectra (5% damping).

validated numerical modelling technique, *p-y* and *t-z* (*q-z*) springs are used to link the soil column to the piles in the lateral and vertical directions, respectively.

4.2. Studied parameters for sensitivity analyses

Table 2 lists the studied fourteen parameters for sensitivity analyses, together with their uncertain properties. These parameters are sorted into structure- and soil-related ones. The structure-related ones can be further categorized into column-associated and pile-associated ones. Also, the structure-related ones can be classified as geometric configurations (H, D, d and S), reinforcement ratios ($\rho_{l\text{-}col}$, $\rho_{s\text{-}col}$, $\rho_{l\text{-}pile}$ and $\rho_{s\text{-}pile}$), and material strengths (f_c, f_y and E_s). Note that bar buckling is not considered in this study since it can be avoid through proper design

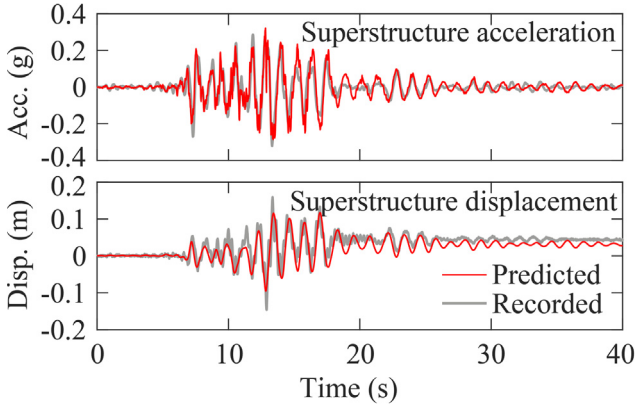

Fig. 8. Model validation: Time histories of superstructure acceleration and displacement.

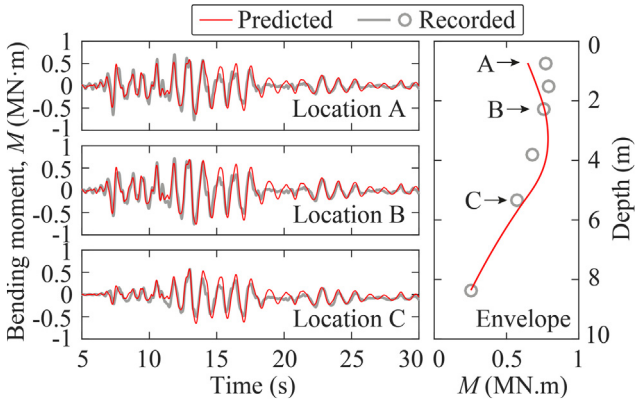

Fig. 9. Model validation: Time histories of pile bending moment at various locations and associated envelope distribution along depth.

[49]. The mean values in Table 2 represent regular constructed modern bridges in practices. Coefficients of variance (COVs) as well as lower and upper bounds of the parameters, which are supposed to be normal distributions, are obtained from literature or assumed according to in-depth communications with experienced engineers, which roughly represent one standard derivation above and below the mean values. There are 1 (mean) + 14 × 2 (lower and upper) = 29 cases for each scour scenario. In total, 29 × 3 = 87 cases are considered. It is worth noting that group efficiency factors are used to represent group effects in the studied 3 × 2 pile-group foundation, as remarked in Table 2. Parameters for constitutive models of the sands (PDMY) are listed in Table 3.

4.3. Considered EDPs and sensitivity of section limit states to parameters

Three EDPs are considered, including the bearing deformation, the peak column curvature and pile curvature. It should be noted that the column drift ratio and pile-cap lateral displacement, which can be conveniently computed, are not appropriate candidates for damage quantifications of bridge columns and piles in scoured or liquefiable ground [57,58], since such ground conditions can significantly increase the flexibility of pile foundations (e.g., remarkable rotations and displacements at pile-caps), thereby affecting capacity values of these two candidates. Moreover, these two candidates cannot capture localized damage to piles. Therefore, these two candidates are not used. Instead, this study adopts the peak curvatures to quantify damage to the single column and piles. For conciseness, merely two damage limit states, slight and complete, are assessed for the considered EDPs. Table 4 lists their capacity values under dead loads, together with the dispersions obtained from literature. Specifically, the capacity values for the

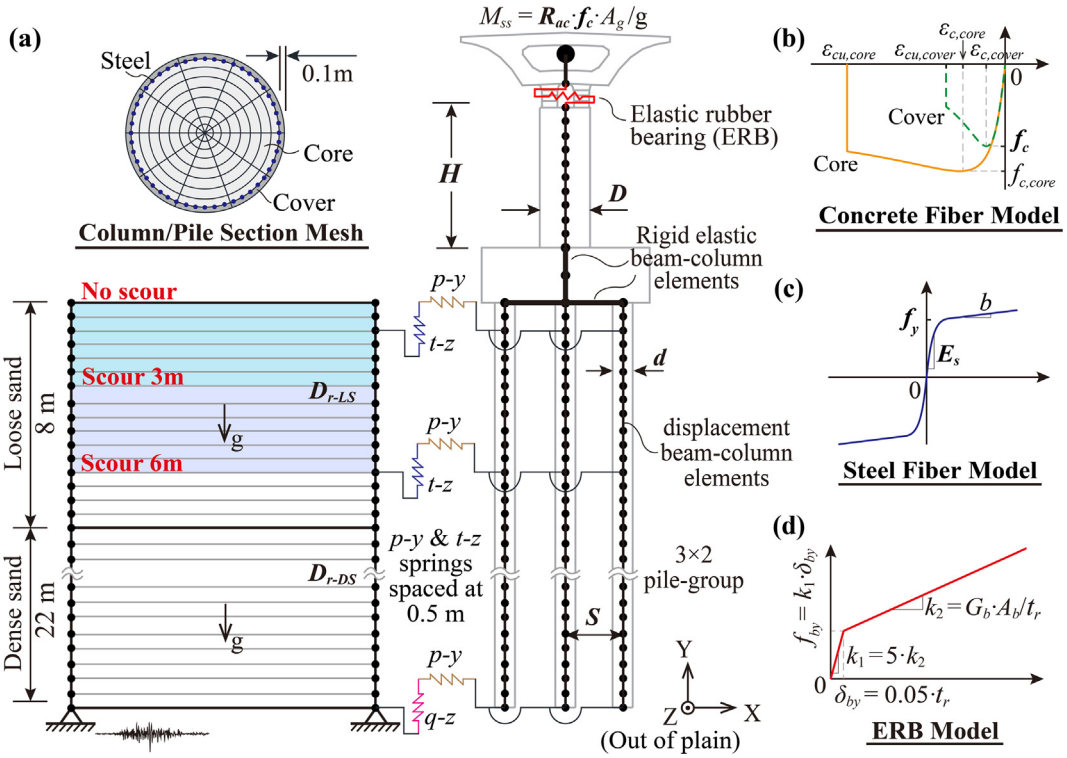

Fig. 10. FE modelling of the soil-bridge system: (a) coupled soil-foundation-bridge model and section mesh, (b) concrete model, (c) steel model and (d) elastic rubber bearing (ERB) model.

bearing deformation refer to a 100% and 250% shear strain regarding the abovementioned 0.07 m-thickness rubber layers of ERBs for the slight and complete damage limit states, respectively. The curvature limit states are obtained from section moment-curvature analyses using zero-section elements in *OpenSees* [26]. The slight damage level corresponds to the first-yield curvature, while the complete damage level refers to the ultimate curvature that is represented by concrete core crushing or rebar snapping, whichever occurs first. Note that for the studied cases, the concrete core crushes always before the rebar snaps. Additionally, it should be noted that the cap-rotation-induced axial load variations during the dynamic analyses are tracked to account for their impacts on the ultimate curvatures, as those performed by the authors in a former study [12]. As for the first-yield curvatures, the impacts of axial load variations appear to be very slight and generally can be neglected [8].

Based on the conventional Tornado diagram approach, Fig. 11 shows the relative sensitivity of the section-relevant parameters on the first-yield and ultimate curvatures of the pile and column sections. For the first-yield curvature (i.e., slight damage limit state), diameters (D and d) are the most sensitive parameters, followed by steel strength parameters (f_y and E_s), column axial compressive ratio (R_{ac}) and longitudinal reinforcement ratios ($\rho_{l\text{-}col}$ and $\rho_{l\text{-}pile}$). It is worth noting that the column diameter (D) has a noticeable impact on the first-yield curvature of the pile section, since it changes axial loads of the pile and thereby acts like R_{ac}. On the contrary, the concrete strength (f_c) and transverse reinforcement ratios ($\rho_{s\text{-}col}$ and $\rho_{s\text{-}pile}$) have no impacts on the first-yield curvature. In terms of the ultimate curvature (i.e., complete damage limit state), by contrast, $\rho_{s\text{-}col}$ and $\rho_{s\text{-}pile}$ are the most sensitive

Table 2
Studied parameters and their uncertain properties.

#	Parameter (Unit)	Description	Mean	COV [Ref.]	Lower	Upper
Structure-related						
1	H (m)	Column height	6.5	26% [50]	4.8	8.2
3	D (m)	Column diameter	2	10% *	1.8	2.2
2	R_{ac} (/)	Column axial compressive ratio	0.1	20% *	0.08	0.12
4	$\rho_{l\text{-}col}$ (/)	Column longitudinal reinforcement ratio	0.015	27% [50]	0.011	0.019
5	$\rho_{s\text{-}col}$ (/)	Column transverse reinforcement ratio	0.005	42% [50]	0.003	0.007
6	d (m)	Pile diameter	1	10% *	0.09	0.11
7	S (m) †	Pile center-to-center distance	3d	15% *	2.5d	3.5d
8	$\rho_{l\text{-}pile}$ (/)	Pile longitudinal reinforcement ratio	0.01	27% [50]	0.007	0.013
9	$\rho_{s\text{-}pile}$ (/)	Pile transverse reinforcement ratio	0.004	42% [50]	0.002	0.006
10	f_c (MPa)	Concrete cover strength	34	18% [51]	28.4	40.6
11	f_y (MPa)	Rebar yielding strength	400	5% [52]	381	420
12	E_s (GPa)	Rebar elastic modulus	200	3.3% [53]	194	207
Soil-related						
13	$D_{r\text{-}LS}$ (/)	Loose sand relative density	0.37	19% [54]	0.30	0.44
14	$D_{r\text{-}DS}$ (/)	Dense sand relative density	0.75	19% [54]	0.61	0.89

* Assumed based on experienced engineering judgements.
† Group efficiency factors = 0.7, 0.8 and 0.9 for S = 2.5d, 3d and 3.5d, respectively [55].

Table 3
Parameters for sand constitutive models (PDMY) in the studied soil-bridge system.

Parameter (Unit)	Loose sand layer			Dense sand layer		
D_r (%)	30 (Lower)	37 (Mean)	44 (Upper)	61 (Lower)	75 (Mean)	89 (Upper)
ρ (ton/m^3)	1.93	1.95	1.96	2.00	2.03	2.07
φ	30.7	32.0	33.1	36.2	38.7	41.2
e	0.772	0.744	0.720	0.652	0.598	0.543
$f_r^{'}$(kPa)	80	80	80	80	80	80
$G_{max,oct}$ (MPa)	48.3	56.7	64.6	88.1	108	130
γ_{max}	0.1	0.1	0.1	0.1	0.1	0.1
B_r (MPa)	129	151	172	235	289	345
d_p	0.5	0.5	0.5	0.5	0.5	0.5
c	0.0452	0.0401	0.0364	0.0283	0.0234	0.0193
d_1	0	0.4	0.4	0.5	0.6	0.8
d_2	0	2	2	3	3	4
Liq_1	10	10	10	7	5	0
Liq_2	0.02	0.01	0.008	0.006	0.003	0
Liq_3	1	1	1	1	1	0

ones, followed by f_c and D. The steel strength parameters (f_y and E_s) are insensitive to the ultimate curvature. In other words, from the slight to complete damage limit states, the sensitivity of transverse reinforcement ratios and concrete strengths increases while the steel strengths decrease.

4.4. Adopted ground motions

To produce reliable fragility curves, a large number of ground motions ought to be used to establish reliable PSDMs. However, massive dynamic analyses are usually time-consuming tasks. Hence, from a view of practice, to make a balance between the reliability and the efficiency, 40 non-pulse-like real ground motions for rock sites, which were selected by Baker et al. [59] as a standardized set of ground motions for seismic analysis of transportation infrastructure in California, are adopted in this study for each case. In light of Gehl et al. [60], 40 dynamic analyses are deemed generally sufficient for deriving a reliable fragility curve using Cloud method, as imposed in this study. In total, $40 \times 87 = 3480$ dynamic analyses are run in this study. The ground motions are input at the base of the soil column, which is supposed to lie on a very firm stratum on top of the bedrock. Fig. 12 shows acceleration spectra of the 40 ground motions, together with the mean spectrum.

5. Characteristic results of the dynamic analyses

5.1. Typical seismic responses

To preliminarily characterize the seismic responses of the studied soil-bridge system under scour and liquefaction effects, this section presents typical responses at individual components of the system with the mean parameters under the 09/21/1999 Chi-chi ground motion recorded at WNT Station (NGA record sequence number 1596).

Fig. 13 compares excess pore pressure developments for the studied scour scenarios, including contour plots across the depth and time, envelopes along the depth and time history responses at soil surfaces. The input acceleration and its Arias intensity (AI) development [61] are plotted as well. It is seen that before liquefaction, buildups of r_u generally follow the tendency of AI development, indicating a good ability of liquefaction prediction for AI. This finding supports former studies that AI is capable of predicting soil liquefaction (e.g. [62,63], among others). As for the impact of scour, increasing the scour depth reduces both the duration and extent of liquefaction (i.e., levels of pore pressure increments). This result is supposed owing to the influence of scour on the stiffness of the soil column, which affects the wave propagation. Further in-depth studies are required to reveal the inherent mechanism, which will be presented in a future paper.

Fig. 14 presents bearing deformation responses across different scour scenarios under the Chi-chi ground motion. The no scour scenario shows the largest peak response, followed by the scour 3 m and 6 m scenarios, successively. This result is owing to the isolation effect induced by the increase of scour depth. Also, for this reason, the scenario of scour 6 m displays less cycles in the time domain (i.e., a larger vibration period) than the scour 3 m scenario and even less than the no scour scenario.

Fig. 15 compares column and pile curvature responses among the studied three scour scenarios under the Chi-chi ground motion. Note that the pile curvature response represents the one, among the 3×2 pile group, that undergoes the most severe damage (hereinafter inclusive). The curvature envelopes in Fig. 15(a) show that the column curvature responses decrease with the increasing scour depths, while the pile curvature counterparts apparently increase. This trend is further reflected by time history responses at the column bottom and the pile head, shown in Fig. 15(b) and (c). These results, together with the above bearing responses, indicate that scour can transfer failure modes of the bridge from the bearing and column bottom to the pile head under this ground motion. From a view of modern design philosophies, this trend is against the capacity design principle that the column should fail before the pile foundation. In other words, the effect of scour is generally detrimental for constructed bridges that were designed

Table 4
Capacity and dispersion (reference) for EDPs at slight and complete damage limit states.

EDP (Unit)	Slight damage		Complete damage	
	Capacity	Dispersion	Capacity	Dispersion
Bearing deformation (m)	0.07	0.79 [56]	0.175	0.66 [56]
Column curvature (1/m)	2.03×10^{-3} *	0.59 [21]	3.32×10^{-2} *	0.65 [21]
Pile curvature (1/m)	4.10×10^{-3} *	0.59 [21]	7.14×10^{-2} *	0.65 [21]

* Curvature capacity values for the case with the mean values of parameters. These values shall vary for cases with the lower and upper bounds of parameters.

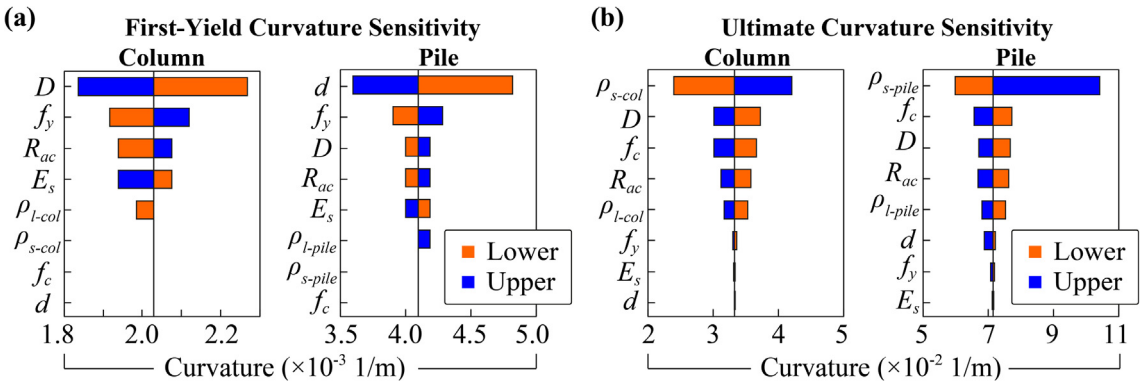

Fig. 11. Sensitivity of parameters on column and pile section curvatures at different limit states: (a) first-yield, and (b) ultimate.

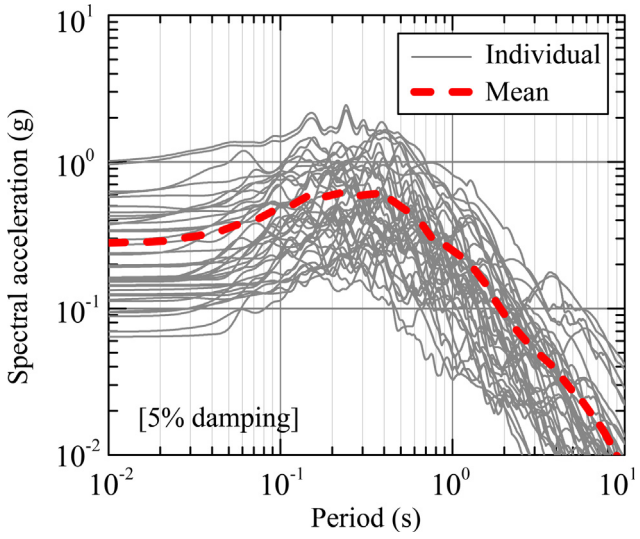

Fig. 12. Acceleration spectra of the adopted 40 ground motions.

following the capacity design principle.

5.2. Fragility curve examples for bridge components

This section shows fragility curve examples that represent impacts of scour depths and parameter variations on probabilities of slight and complete damage states to individual components of bridges. In light of former studies on optimal IMs for probabilistic seismic demand modelling of bridges in liquefiable ground (e.g., [41,64,65]), peak ground velocity (PGV) is adopted for fragility analyses.

Based on the model with the mean parameters, Fig. 16 presents the impact of scour depth on fragility curves of the studied bridge components at their slight and complete damage limit states. From Fig. 16(a) and (b), the larger scour depth, the lower damage probability, implying that scour has beneficial effects on the bearing and column by providing a way of base isolation (i.e., increasing the flexibility of the bridge and thereby elongating its fundamental period). However, the increase of scour depth apparently increases the probability of damage to the pile foundation, meaning that scour has a detrimental effect on the pile foundation, which should be mainly attributed to the stronger soil-pile kinematic interactions due to the scour-induced flexibility increment in the pile foundation in this study. More specifically, scour has two-fold effects on pile responses: (1) elongating periods of bridges, which can usually reduce the responses; (2) increasing lateral deflections of piles, which inevitably increases resistances provided by soils. The increased soil resistances in turn counteract the reduced responses due to the elongation of periods. Therefore, the final effect of scour on the fragility of piles depends on which effect dominates. In addition, the different tendencies of fragility curves for different components across the scour scenarios verifies the above inference that scour can significantly vary failure modes of bridges in liquefiable soils via transferring the damage positions from bearings and columns to piles. This finding is consistent with former numerical and experimental studies on the impact of scour on the seismic behavior of bridges in nonliquefiable soils [7,57,66].

Before presenting sensitivity rankings of the studied parameters, Figs. 17 and 18 indicatively show the impact of loose sand relative

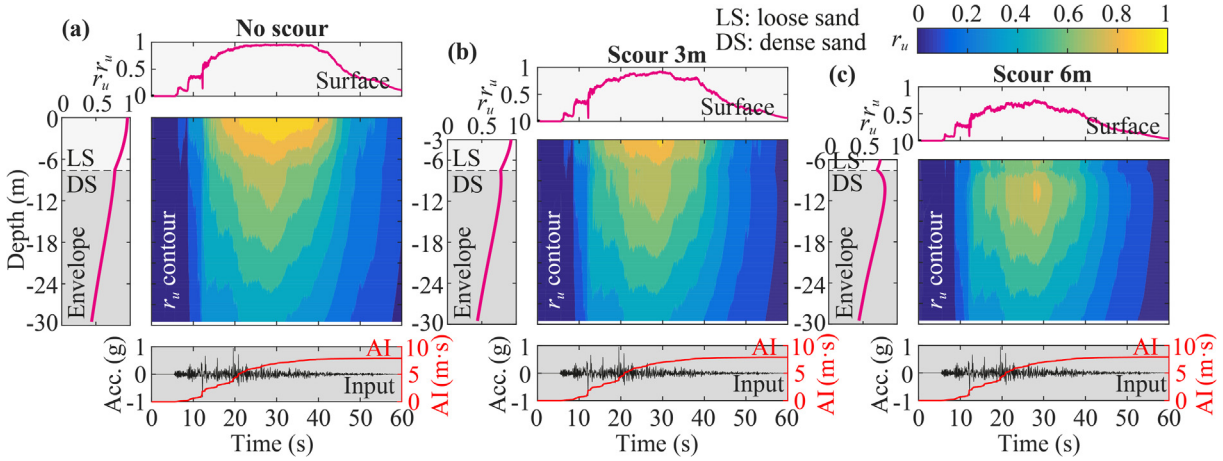

Fig. 13. Excess pore pressure developments (contour plots across the depth and time, envelope and time history at surface) for different scour scenarios under the 1999 Chi-chi earthquake.

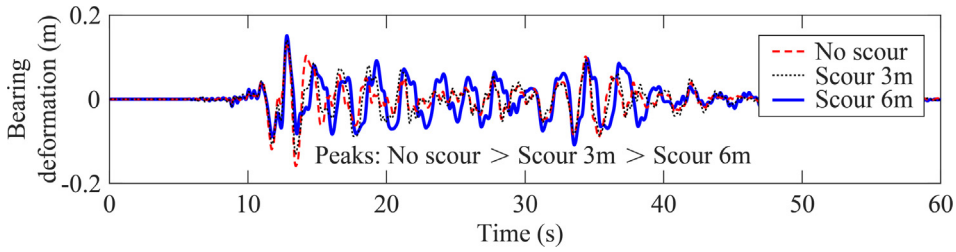

Fig. 14. Bearing deformations for different scour scenarios under the 1999 Chi-chi earthquake.

density ($D_{r\text{-}LS}$) on the fragility of pile and column, respectively, across different scour scenarios. A global inspection of these two figures shows that gaps of fragility curves between the cases with the upper and lower bounds appear to decrease with the increase of scour depth, which indicates that scour tends to decrease the sensitivity of $D_{r\text{-}LS}$ in fragility assessment of the pile and column. More specifically, for the pile in Fig. 17, a higher $D_{r\text{-}LS}$ triggers a lower damage probability, regardless of different scour depths or damage limit states, which means that densifying the upper liquefiable loose sand layer can improve the seismic performance of pile foundation by mitigating the liquefaction hazard. This theory has been widely applied in practices for ground improvements [67]. By contrast, Fig. 18 shows that densifying the loose sand layer increase the damage probability of the column, regardless of damage limit states and scour depths, because a densified ground can provide a stiffer boundary condition that reduces the flexibility of the column, thereby increasing its demand. Nevertheless, this trend that the damage probability of the column increases while that of the pile decreases is practically acceptable, since it abides the capacity design principle to protect the foundation. Therefore, densifying the upper liquefiable loose sand layer is a desirable solution in practices.

6. Sensitivity analyses results

This section presents fragility-based Tornado diagram results for absolute and relative sensitivity rankings of the parameters in terms of the monitored EDPs across different scour scenarios. Results at the slight damage limit states across different scour scenarios are adopted to show the effect of scour depth. Results of the scour 3 m scenario across the slight and complete damage limit states are then used to present the effect of damage limit state. Additionally, recommendations on using relatively larger or smaller parameters for improving the seismic performance are discussed to provide preliminary insights into retrofits and designs of bridges in liquefiable ground considering scour potentials.

6.1. Effects of scour depths on sensitivity rankings of the parameters

Figs. 19 to 21 present the effect of scour depth on sensitivity rankings of the parameters for the fragility assessment of bearing, column and pile, respectively. Note that to assess the variation of global absolute sensitivity of the parameters (i.e., the larger R_{IM} value, the higher absolute sensitivity) across the studied scour scenarios, identical widths are set for the horizontal axes of different scour scenarios. A quick inspection from the no scour to scour 6 m scenarios shows that scour generally increases the absolute sensitivity for the bearing and column (Figs. 19 and 20), while it apparently decreases that for the pile (Fig. 21). Recalling that scour can decrease the damage probability of the bearing and column, while increases that of the pile (see Fig. 16), it can be concluded that the absolute sensitivity of these parameters tends to be higher for fragility curves showing lower damage probabilities. In this regard, it is reasonable to speculate that the absolute sensitivity of parameters for seismic performance assessment of bridge components at complete damage limit states should be much higher than that at slight damage limit states (further interpreted later in this paper).

Besides, backgrounds are illustrated in Figs. 19 to 21 to highlight the noted transfer tendencies of relative sensitivity across the studied scour scenarios (i.e., the upper position in Tornado diagram, the higher relative sensitivity). Specifically, parameters with bright backgrounds and black fonts represent those exhibiting decreasing tendencies of relative sensitivity across the scour scenarios, while parameters with dark backgrounds and white fonts stand for those showing increasing tendencies. From Fig. 19, axial compressive ratio (R_{ac}) and concrete strength (f_c) are stably the most sensitive parameters for the fragility assessment of bearing, disregarding scour depths. This is because these

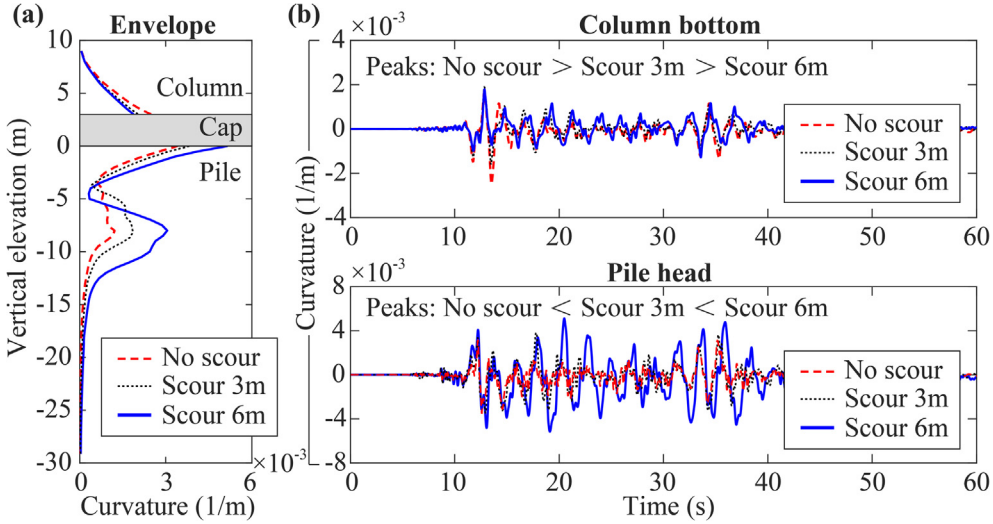

Fig. 15. Column and pile curvatures for different scour scenarios under the 1999 Chi-chi earthquake: (a) envelope and (b) column bottom and pile head time history responses.

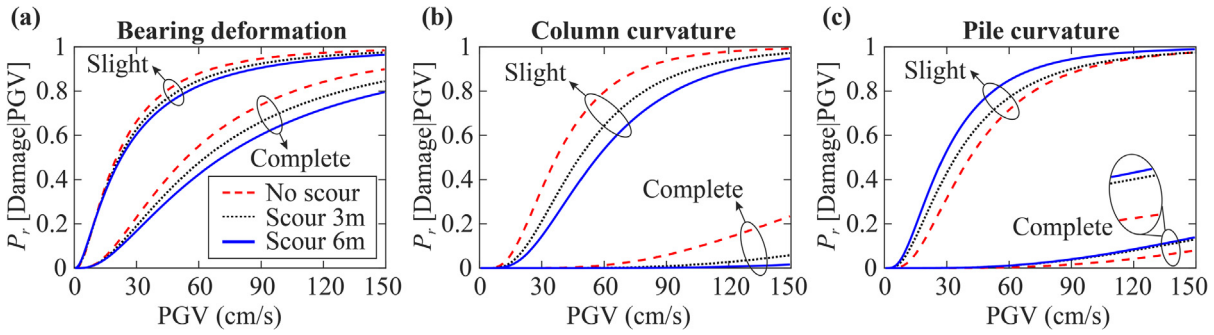

Fig. 16. Impacts of scour depths on the fragility of different EDPs: (a) bearing deformation, (b) column curvature, and (c) pile curvature.

two parameters dominate the superstructure mass (i.e., $M_{ss} = R_{ac} f_c' A_g /g$, see Fig. 10 or Section 4.1), which represents the inertial force that triggers the bearing deformation. Column height (H), which is the most sensitive one for the no scour scenario, becomes less and less sensitive with the increases of scour depths. This is because scour significantly increases the lateral flexibility of the bridge, which thereby reduces the influence of H that characterize the flexibility before scour. By contrast, column diameter (D) generally shows increasing relative sensitivity with the increasing scour depths. Also, pile-associated parameters such as diameter (d) and longitudinal reinforcement ratio ($\rho_{l\text{-}pile}$) exhibit upgrading tendencies across the scour scenarios. In addition, the soil-related parameters (i.e., loose and dense sand relative densities, $D_{r\text{-}LS}$ and $D_{r\text{-}DS}$) apparently show decreasing relative sensitivity. This phenomenon is attributed to the scour-induced decrease of loose sand layer, which in turn reduces the contribution of the loose sand layer to the performance assessment of bridge components. On the other hand, steel parameters (yielding strength, f_y and elastic modulus, E_s) and transverse reinforcement ratios of the column and pile ($\rho_{s\text{-}col}$ and $\rho_{s\text{-}pile}$) are generally the least sensitive parameters for the slight damage limit state, disregarding scour depths.

For Tornado diagram results of the column in Fig. 20, column-associated parameters such as H, D and $\rho_{l\text{-}col}$ are generally the most sensitive ones across the three scour scenarios. By contrast, R_{ac}, which is practically the most sensitive parameter for the bearing, becomes much less sensitive for the column, which may be because that the difference of column curvature response between the cases with lower and upper bounds of R_{ac} counteracts that of the curvature capacity of the column section. In addition, the relative sensitivity of R_{ac} and soil relative densities ($D_{r\text{-}LS}$ and $D_{r\text{-}DS}$) shows a decreasing trend across the scour scenarios. By contrast, pile-associated parameters such as d, $\rho_{l\text{-}pile}$ and pile center-to-center distance (S) exhibit upgrading relative sensitivity with the increase of scour depth. On the other hand, material strength parameters (f_c, f_y and E_s) and transverse reinforcement ratios ($\rho_{s\text{-}col}$ and $\rho_{s\text{-}pile}$) are generally insensitive parameters for the seismic performance assessment of column, regardless of scour depths.

As for the sensitivity results of the pile (Fig. 21), although the top three sensitive parameters vary across the scour scenarios, the pile diameter (d) is generally the most sensitive one. Regarding the tendencies of relative sensitivity across the scour scenarios, some column-associated parameters (H, D and $\rho_{l\text{-}col}$) and the soil-related ones ($D_{r\text{-}LS}$ and $D_{r\text{-}DS}$) show decreasing tendencies, while the pile-associated ones (e.g., d, $\rho_{l\text{-}pile}$ and S) generally display increasing tendencies. On the other hand, similar to the column, material strength parameters (f_c, f_y and E_s) and transverse reinforcement ratios ($\rho_{s\text{-}col}$ and $\rho_{s\text{-}pile}$) are insensitive parameters for the pile.

Gathering the above sensitivity results for different components at the slight damage limit states, it can be summarized that across the studied scenarios, R_{ac}, f_c and H are noticeably sensitive parameters for the bearing, H, D and $\rho_{l\text{-}col}$ are the top sensitive parameters for the column, while d is the most sensitive parameter for the pile. On the contrary, transverse reinforcement ratios ($\rho_{s\text{-}col}$ and $\rho_{s\text{-}pile}$) and material strength parameters (f_c, f_y and E_s) are insensitive ones for the fragility assessment of bridge components at the slight damage limit state. Moreover, increasing the scour depth can downgrade the relative sensitivity of column-associated and soil-related parameters, while upgrade that of the pile-associated ones. In other words, for fragility-based seismic retrofits and designs of bridges in liquefiable soils, e.g., considering slight damage limit states of bridge components, more attentions should be paid to pile-associated parameters, such as d, $\rho_{l\text{-}pile}$ and S, when accounting for scour potentials.

6.2. Effects of damage limit states on sensitivity rankings of the parameters

Another issue of interest is the influence of damage limit states. Fig. 22 compares the sensitivity rankings of the studied parameters at the slight and complete damage limit states for different bridge components, represented by the results of scour 3 m scenario. Widths of the horizontal axes for the complete damage limit states are much larger than those for the slight damage limit state, which verifies the above speculation that the absolute sensitivity for the complete damage limit states is much higher than that for the slight damage limit states. This may be partially attributed to the higher absolute sensitivity of parameters for the section ultimate curvatures compared to the first-yield curvatures, as shown above in Fig. 11, where widths of the horizontal

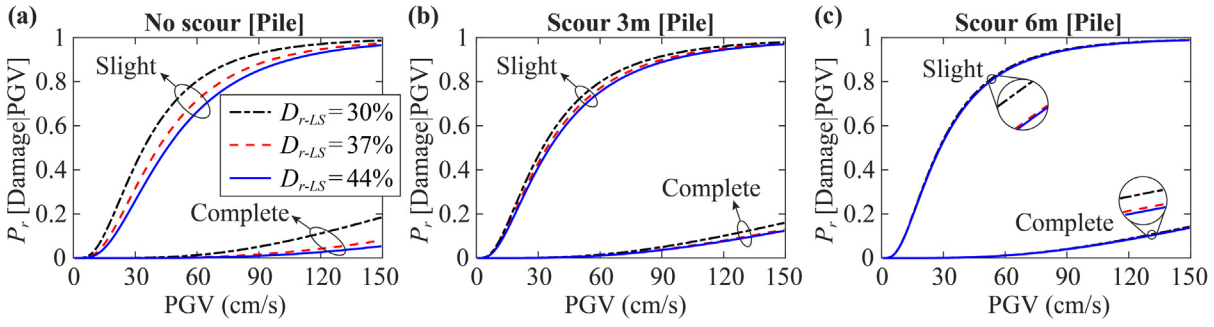

Fig. 17. Impacts of loose sand relative density ($D_{r\text{-}LS}$) on the fragility of pile across different scour scenarios: (a) no scour, (b) scour 3 m, and (c) scour 6 m.

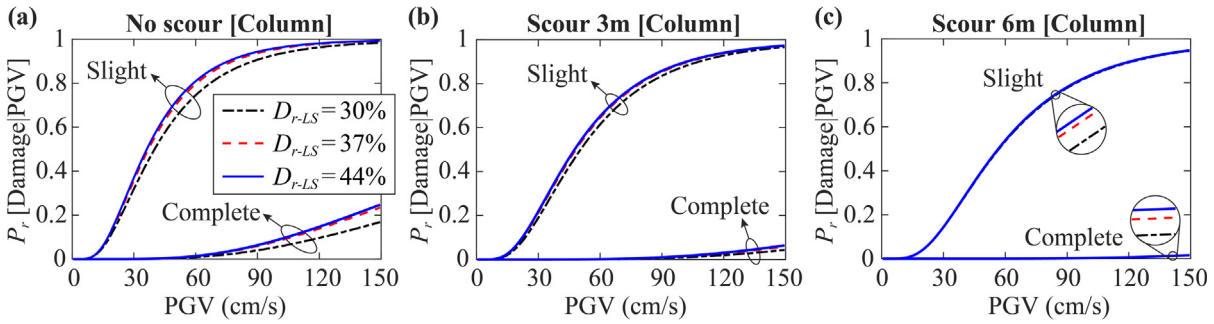

Fig. 18. Impacts of loose sand relative density (D_{r_LS}) on the fragility of column across different scour scenarios: (a) no scour, (b) scour 3 m, and (c) scour 6 m.

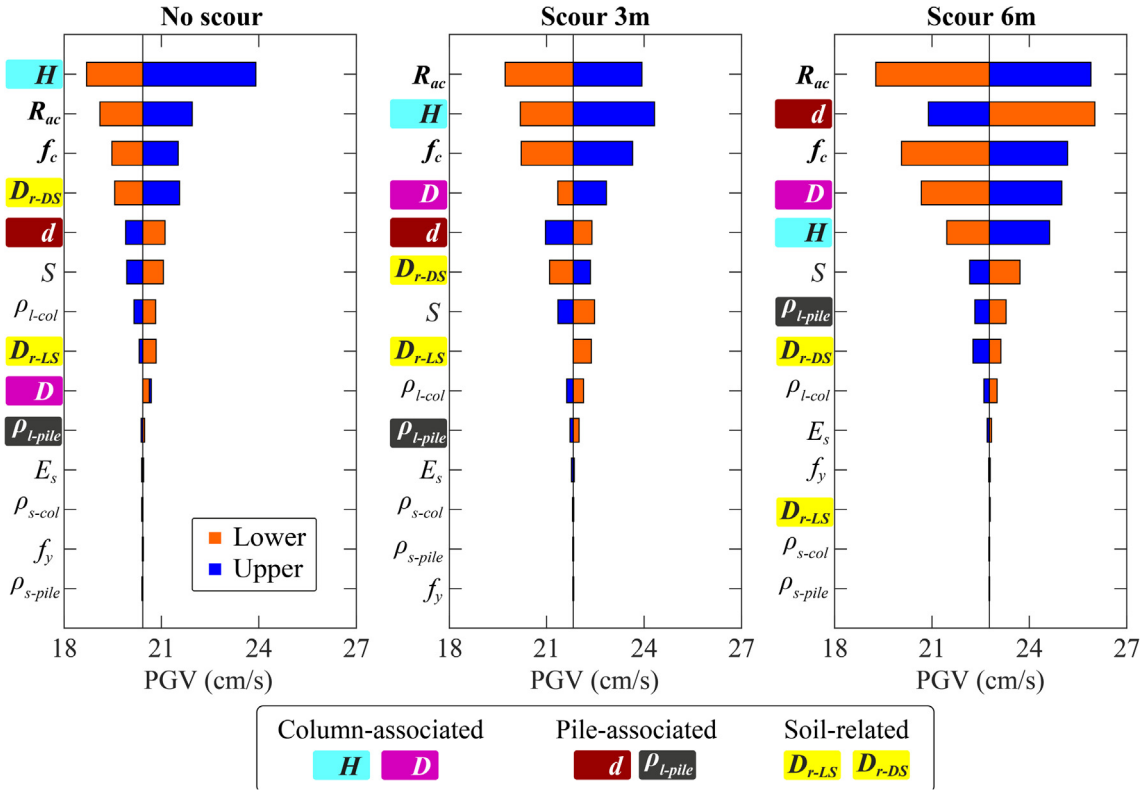

Fig. 19. Effects of scour depths on sensitivity rankings of parameters for bearing deformation.

axes for the ultimate curvatures are remarkably larger than those for the first-yield curvatures.

In terms of the relative sensitivity, from Fig. 22(a), the bearing results does not show significant changes for different damage limit states, although few parameters in Tornado diagram slightly change positions with their adjacent ones. By contrast, noted variations are observed for some parameters in the results of column and pile, although the most sensitive ones (i.e., generally *H*, *D* and *d*) are not remarkably influenced by the different limit states. More specifically, for the column (Fig. 22(b)), the relative sensitivity of f_y significantly downgrades from the slight to the complete damage limit states, while that of $\rho_{s\text{-}col}$ dramatically upgrades. This is because that f_y is a very sensitive parameter for the section capacity model at the slight damage limit state, while $\rho_{s\text{-}col}$ is the most sensitive parameter for its complete damage limit state (see Fig. 11). As for the pile (Fig. 22(c)), similar transfer trends of f_y and $\rho_{s\text{-}pile}$ are witnessed for the same reason above. Besides, $\rho_{l\text{-}pile}$, which is the third most sensitive parameter for the slight damage limit state of pile curvature turns to an insensitive one for the complete damage limit state, while on the contrary, the insensitive parameter, f_c, for the slight damage limit state exhibits an influential role for the complete damage limit state. This result is attributed to the fact that the slight damage limit state is dominated by the yielding of rebar (relevant to $\rho_{l\text{-}pile}$), while the complete damage limit state is controlled by the crushing of concrete core (relevant to f_c). In addition, it should be noted that the relative sensitivity of the upgrading parameters for the complete damage limit state (i.e., $\rho_{s\text{-}col}$, $\rho_{s\text{-}pile}$ and f_c) is generally stable across the studied scour scenarios (not presented for conciseness). Moreover, it is worth noting that the abovementioned scour-induced transfer tendencies of relative sensitivity at the slight damage limit state are practically observed at the complete damage limit state.

6.3. Preliminary recommendations for seismic performance improvements

Recalling that the bar in the right side of Tornado diagram represent the case with a lower damage probability, thereby indicating a better performance for that parameter using the lower or upper bound. Following this criterion, bars in Figs. 19 to 22 are assessed to provide preliminary recommendations for seismic performance improvements of the bridge components. Table 5 lists the results, in which the check mark (✓) represents that increasing this parameter from the mean to the upper bound can improve the seismic performance of the

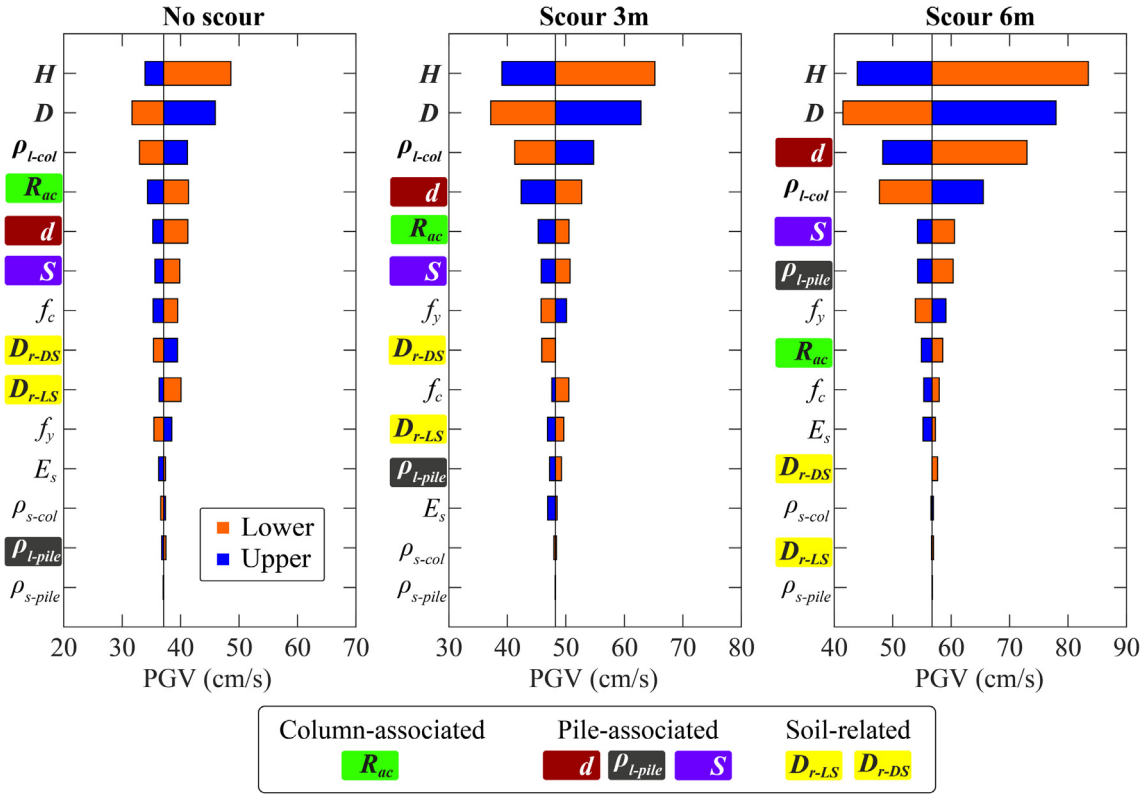

Fig. 20. Effects of scour depths on sensitivity rankings of parameters for column curvature.

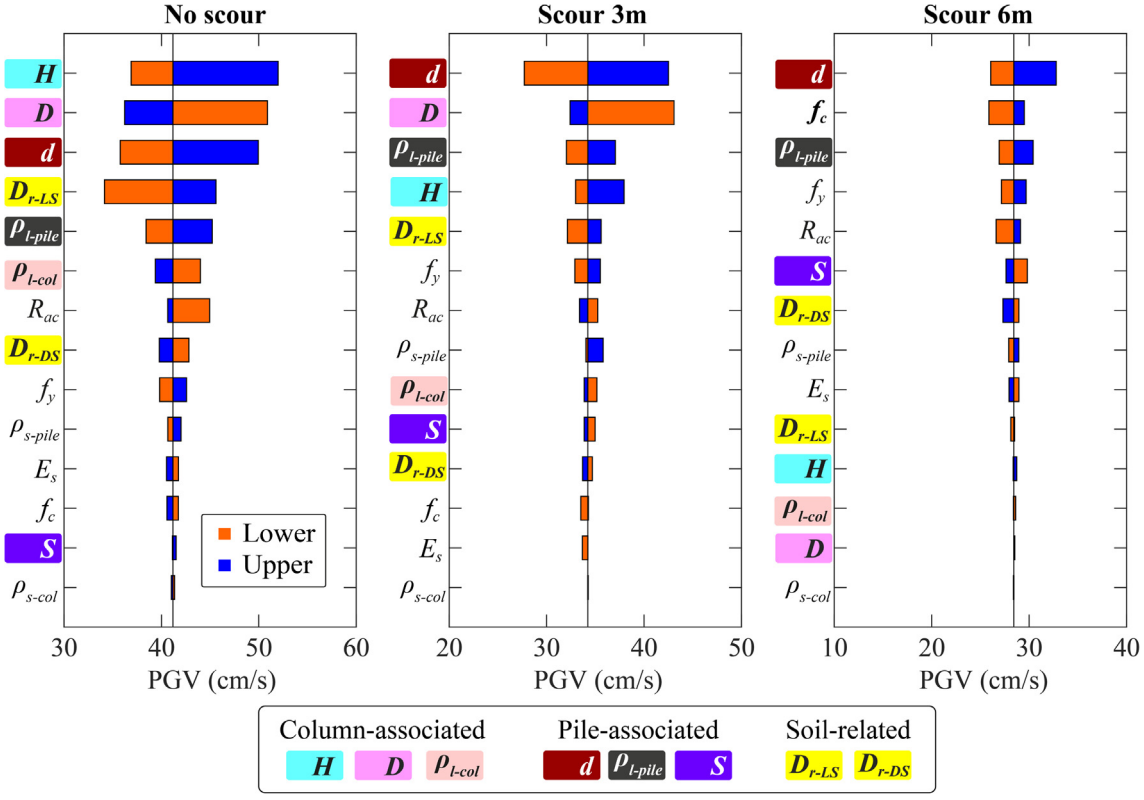

Fig. 21. Effects of scour depths on sensitivity rankings of parameters for pile curvature.

component (i.e., by reducing the damage probability of the fragility curve), while the cross mark (✗) refers to that increasing the parameter to the upper bound degrades the performance; in other words, decreasing it to the lower bound may improve the performance. In addition, the slash mark (/) indicates that this parameter is generally too insensitive to provide a noted conclusion.

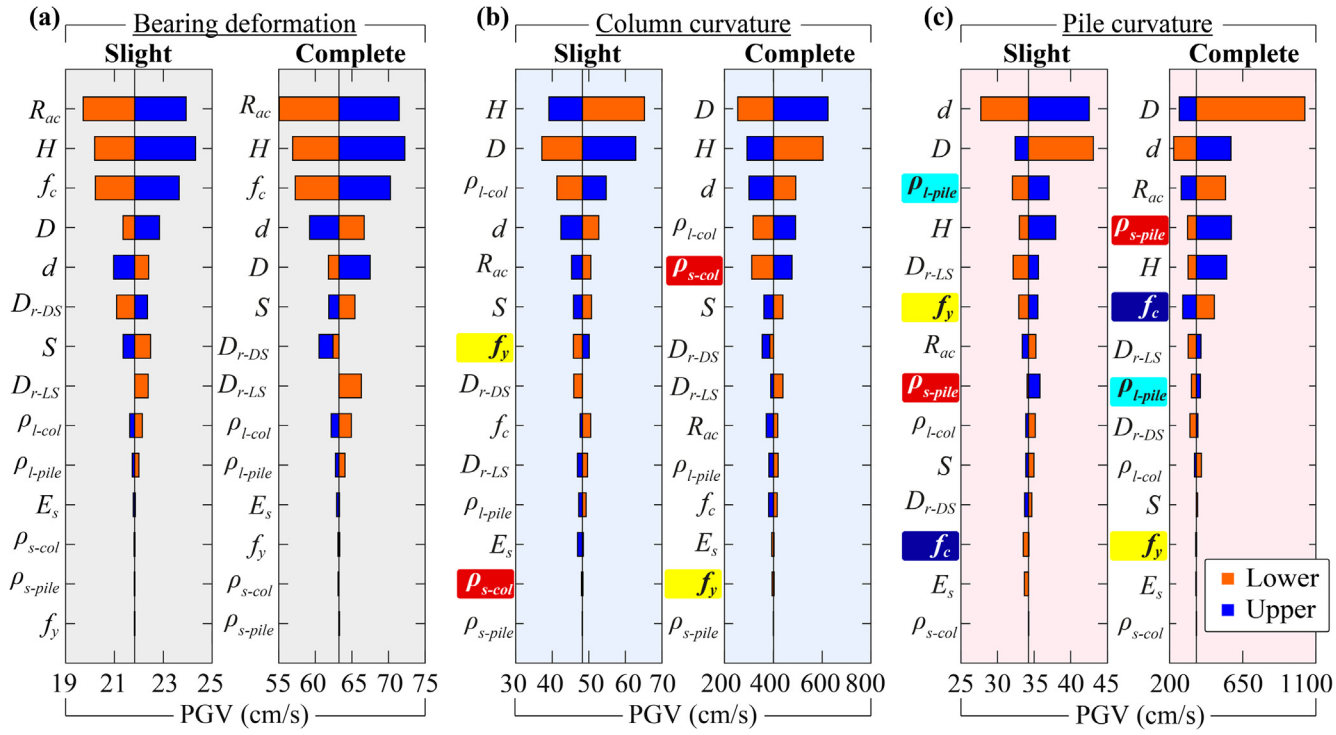

Fig. 22. Effects of damage limit states on relative sensitivity of parameters in the scenario scour 3 m for different EDPs: (a) bearing deformation, (b) column curvature, and (c) pile curvature.

For the individual components in Table 5, it is found that within the studied parameter bounds, relatively larger H, D, R_{ac} and f_c as well as smaller d and S can improve the seismic performance of the bearing. As for the column, relatively larger D, reinforcement ratios ($\rho_{l\text{-}col}$ and $\rho_{s\text{-}col}$), f_y as well as smaller H, R_{ac}, d, S, f_c and $D_{r\text{-}LS}$ can improve the performance. For the pile foundation, larger H, d, $\rho_{l\text{-}pile}$, $\rho_{s\text{-}pile}$, f_y and $D_{r\text{-}LS}$ as well as smaller D, R_{ac}, S are beneficial to its seismic performance.

In terms of the individual parameters, compromises should be achieved when determining H, D, R_{ac}, d, f_c and $D_{r\text{-}LS}$ in seismic designs or retrofits of bridges subjected to scour and liquefaction potentials, since increasing or reducing these parameters cannot bring consistent beneficial effects to all the studied bridge components. More specifically, using a larger d can improve the performance of the foundation, while it brings detrimental effects to the column and bearing. However, this trend follows the modern capacity design principle that columns should fail before pile foundations. Also, a relatively smaller D and larger H and $D_{r\text{-}LS}$ can protect the pile foundation via increasing damage probabilities of the column and/or bearing. In addition, a larger f_c tends to reduce the damage probability of the pile foundation in the scour 6 m scenario (see Fig. 21), although it may provide detrimental effects to the column. On the other hand, using a smaller S (i.e., 2.5d as compared to 3d) helps to improve the performance of the pile, column and bearing together. Moreover, adopting greater $\rho_{l\text{-}col}$, $\rho_{s\text{-}col}$, $\rho_{l\text{-}pile}$, $\rho_{s\text{-}pile}$ and f_y can generally improve the performance of their corresponding components. Therefore, larger pile diameter, column height, longitudinal/transverse reinforcement ratios and RC material strengths as well as smaller column diameter and pile center-to-center space are recommended for modern design philosophies accounting for the mitigation of scour and liquefaction effects on the seismic performance of pile-supported bridges.

7. Conclusions

This paper aims to identify sensitivity rankings of parameters for seismic performance assessment of pile-group-supported bridges in liquefiable soils undergoing scour potentials. To this end, a fragility-

Table 5
Improvements or degradations of the seismic performance of bridge components by increasing the parameters to the upper bounds.

Increase of parameter	Description	Seismic performance improved?		
		Bearing	Column	Pile
H	Column height	✓	✗	✓
D	Column diameter	✓	✓	✗
R_{ac}	Column axial compressive ratio	✓	✗	✗
$\rho_{l\text{-}col}$	Column longitudinal reinforcement ratio	/	✓	/
$\rho_{s\text{-}col}$	Column transverse reinforcement ratio	/	✓	/
d	Pile diameter	✗	✗	✓
S	Pile center-to-center distance	✗	✗	✗
$\rho_{l\text{-}pile}$	Pile longitudinal reinforcement ratio	/	/	✓
$\rho_{s\text{-}pile}$	Pile transverse reinforcement ratio	/	/	✓
f_c	Concrete cover strength	✓	✗	/
f_y	Rebar yielding strength	/	✓	✓
E_s	Rebar elastic modulus	/	/	/
$D_{r\text{-}LS}$	Loose sand relative density	/	✗	✓
$D_{r\text{-}DS}$	Dense sand relative density	/	/	/

based Tornado diagram method is proposed for sensitivity analyses. Fourteen structure- and soil-related parameters, which are supposed to follow normal distributions, are studied to rank the sensitivity across different scenarios with scour depths of 0 m, 3 m and 6 m. 16th and 84th percentiles of the parameters are adopted as the lower and upper bounds for the sensitivity analyses. Experimentally validated soil-foundation-bridge FE models are built to perform fragility analyses using a set of 40 real ground motions. Monitored EDPs include the bearing deformation, column curvature and pile curvature with the consideration of their slight and complete damage limit states. Main findings are as below.

(1) Regarding fragility assessment at slight damage limit states, it is found that axial compressive ratio, column height and concrete strength are generally the most sensitive parameters for the bearing. As for the column, its height, diameter and longitudinal reinforcement ratio generally occupy the top three positions in Tornado diagrams, representing the most significant sensitivity. In terms of the pile foundation, pile diameter is the most sensitive one.
(2) Most of the abovementioned sensitive parameters are slightly influenced by the effect of scour. However, increasing scour depths does downgrade the relative sensitivity of column-associated (e.g., column height and axial compressive ratio) and soil-related ones (i.e., loose and dense sand relative densities), while upgrade the pile-associated ones such as diameter, longitudinal reinforcement ratio and pile center-to-center distance.
(3) The effect of damage limit state (slight versus complete) hardly affects the relative sensitivity of parameters for fragility assessment of the bearing. As for the column and pile, this effect hardly changes the most sensitive parameters. However, the relative sensitivity of transverse reinforcement ratios is notedly upgraded while steel yielding strength is remarkably downgraded for the complete damage limit states of the column and pile, as compared to their slight damage limit states. In addition, the relative sensitivity of concrete strength is obviously upgraded while the longitudinal reinforcement ratio is remarkably downgraded for the complete damage limit state of the pile.
(4) On the other hand, steel strength parameters and column/pile transverse reinforcement ratios are insensitive parameters for the bearing performance assessment, while steel elastic modulus is the insensitive parameter for the column and pile, disregarding different scour depths or damage limit states.
(5) From the view of modern design philosophies such as the capacity design principle, designs or retrofits of bridges using larger pile diameter, column height, longitudinal/transverse reinforcement ratios and RC material strengths, together with smaller column diameter and pile center-to-center distance are recommended for the purpose of mitigating scour and liquefaction effects on the seismic performance of pile foundations.

It is worth noting that the conclusions drawn in this study are based on the considered lower and upper bounds of the studied parameters and should not be generalized to bridges that have vastly different soil profiles, structural configurations and ground motion types from this study, i.e., regular multi-span RC bridges with fairly uniform bents, each composed by a single column and a 3 × 2 pile foundation embedded into liquefiable ground that is subjected to scour and non-pulse-like ground motions in the transverse direction. The above findings can provide significant insights on the optimization of retrofits/designs of existing/new bridges in liquefiable soils considering scour effects. This study can also aid in expanding the framework for performance-based assessment of bridges under combined effects of multiple hazards. Future studies will explore other types of bridges subjected to hazards in both the transverse and longitudinal directions.

Acknowledgement

This work is supported by China Postdoctoral Science Foundation [grant numbers 2018M640448 and 2019T120380] and National Nature Science Foundation of China [grant number51778469]. These supports are gratefully acknowledged.

Appendix A. Supplementary material

Supplementary data to this article can be found online at https://doi.org/10.1016/j.engstruct.2019.109427.

References

[1] Deng L, Wang W, Yu Y. State-of-the-art review on the causes and mechanisms of bridge collapse. J Perform Constr Facil 2016;30(2):04015005. https://doi.org/10.1061/(ASCE)CF.1943-5509.0000731.
[2] Wardhana K, Hadipriono FC. Analysis of recent bridge failures in the United States. J Perform Constr Facil 2003;17(3):144–50. https://doi.org/10.1061/(ASCE)0887-3828(2003) 17:3(144).
[3] Cubrinovski M, Winkley A, Haskell J, Palermo A, Wotherspoon L, Robinson K, et al. Spreading-induced damage to short-span bridges in Christchurch, New Zealand. Earthq Spectra 2014;30(1):57–83. https://doi.org/10.1193/030513EQS063M.
[4] Buckle I, Hube M, Chen G, Yen WH, Arias J. Structural performance of bridges in the offshore maule earthquake of 27 February 2010. Earthq Spectra 2012;28(Suppl. 1):533–52. https://doi.org/10.1193/1.4000031.
[5] Brandenberg SJ, Boulanger RW, Kutter BL, Chang D. Behavior of pile foundations in laterally spreading ground during centrifuge tests. J Geotech Geoenviron Eng 2005;131(11):1378–91. https://doi.org/10.1061/(ASCE)1090-0241(2005) 131:11(1378).
[6] Liu X, Wang R, Zhang J-M. Centrifuge shaking table tests on 4 × 4 pile groups in liquefiable ground. Acta Geotech 2018;13(6):1405–18. https://doi.org/10.1007/s11440-018-0699-5.
[7] Wang S, Liu K, Chen C, Chang K. Experimental investigation on seismic behavior of scoured bridge pier with pile foundation. Earthq Eng Struct Dyn 2015;44(6):849–64. https://doi.org/10.1002/eqe.2489.
[8] Wang X, Ye A, He Z, Shang Y. Quasi-static cyclic testing of elevated RC pile-cap foundation for bridge structures. J Bridg Eng 2016;21(2):04015042. https://doi.org/10.1061/(ASCE)BE.1943-5592.0000797.
[9] Liu Yu-Ting, Tong Jian-Hua, Lin Yiching, Lee Tsung-Han, Chang Chia-Feng. Real-time bridge scouring safety monitoring system by using mobile wireless technology. Fourth Int. Conf. Genet. Evol. Comput., Shenzhen, China: IEEE 2010. p. 501–4. https://doi.org/10.1109/ICGEC.2010.131.
[10] Cheng Z, Jeremić B. Numerical modeling and simulation of pile in liquefiable soil. Soil Dyn Earthq Eng 2009;29(11–12):1405–16. https://doi.org/10.1016/j.soildyn.2009.02.008.
[11] Wang X, Luo F, Su Z, Ye A. Efficient finite-element model for seismic response estimation of piles and soils in liquefied and laterally spreading ground considering shear localization. Int J Geomech 2017;17(6):06016039. https://doi.org/10.1061/(ASCE)GM.1943-5622.0000835.
[12] Blanco G, Ye A, Wang X, Goicolea JM. Parametric pushover analysis on elevated RC pile-cap foundations for bridges in cohesionless soils. J Bridg Eng 2019;24(1):04018104. https://doi.org/10.1061/(ASCE)BE.1943-5592.0001328.
[13] Klinga JV, Alipour A. Assessment of structural integrity of bridges under extreme scour conditions. Eng Struct 2015;82:55–71. https://doi.org/10.1016/j.engstruct.2014.07.021.
[14] Aygün B, Dueñas-Osorio L, Padgett JE, DesRoches R. Efficient longitudinal seismic fragility assessment of a multispan continuous steel bridge on liquefiable soils. J Bridg Eng 2011;16(1):93–107. https://doi.org/10.1061/(ASCE)BE.1943-5592.0000131.
[15] Wang X, Ye A, Shang Y, Zhou L. Shake-table investigation of scoured RC pile-group-supported bridges in liquefiable and nonliquefiable soils. Earthq Eng Struct Dyn 2019:1–21. https://doi.org/10.1002/eqe.3186. doi:10.1002/eqe.3186.
[16] Shang Y, Alipour A, Ye A. Selection of input motion for seismic analysis of scoured pile-supported bridge with simplified models. J Struct Eng 2018;144(8):04018099. https://doi.org/10.1061/(ASCE)ST.1943-541X.0002067.
[17] Padgett JE, DesRoches R. Sensitivity of seismic response and fragility to parameter uncertainty. J Struct Eng 2007;133(12):1710–8. https://doi.org/10.1061/(ASCE)0733-9445(2007) 133:12(1710).
[18] Choe D-E, Gardoni P, Rosowsky D. Closed-form fragility estimates, parameter sensitivity, and Bayesian updating for RC columns. J Eng Mech 2007;133(7):833–43. https://doi.org/10.1061/(ASCE)0733-9399(2007)133:7(833).
[19] Kwon O-S, Elnashai A. The effect of material and ground motion uncertainty on the seismic vulnerability curves of RC structure. Eng Struct 2006;28(2):289–303. https://doi.org/10.1016/j.engstruct.2005.07.010.
[20] Brandenberg SJ, Kashighandi P, Zhang J, Huo Y, Zhao M. Sensitivity study of an Older-Vintage Bridge subjected to lateral spreading. Geotech. Earthq. Eng. Soil Dyn. IV, Reston, VA: ASCE. 2008.
[21] Padgett JE, Ghosh J, Dueñas-Osorio L. Effects of liquefiable soil and bridge modelling parameters on the seismic reliability of critical structural components. Struct

Infrastruct Eng 2010;9(1):59–77. https://doi.org/10.1080/15732479.2010.524654.
[22] Wang X, Ye A, Luo F. Sesimic response sensitivity analysis of pile supported bridge structures in liquefiable ground. Gongcheng Lixue/Eng Mech 2016;33(8):132–40. https://doi.org/10.6052/j.issn.1000-4750.2015.01.0022.
[23] Bybordiani M, Kazemzadeh Azad S. Optimum design of steel braced frames considering dynamic soil-structure interaction. Struct Multidiscip Optim 2019. https://doi.org/10.1007/s00158-019-02260-4.
[24] Cornell CA, Jalayer F, Hamburger RO, Foutch DA. Probabilistic basis for 2000 SAC federal emergency management agency steel moment frame guidelines. J Struct Eng 2002;128(4):526–33. https://doi.org/10.1061/(ASCE)0733-9445(2002)128:4(526).
[25] Wilson DW. Soil-pile-superstructure interaction in liquefying sand [Ph.D. thesis]. Davis: University of California; 1998.
[26] McKenna F. OpenSees: A framework for earthquake engineering simulation. Comput Sci Eng 2011;13(4):58–66. https://doi.org/10.1109/MCSE.2011.66.
[27] Yang Z. Numerical modeling of earthquake site response including dilation and liquefaction [Ph.D. thesis]. Columbia University; 2000.
[28] Wang Z, Dueñas-Osorio L, Padgett JE. Seismic response of a bridge-soil-foundation system under the combined effect of vertical and horizontal ground motions. Earthq Eng Struct Dyn 2013;42(4):545–64. https://doi.org/10.1002/eqe.2226.
[29] Boulanger RW, Kutter BL, Brandenberg SJ, Singh P, Chang D. Pile foundations in liquefied and laterally spreading ground during earthquakes: centrifuge experiments and analyses. Sacramento, CA, Davis: University of California; 2003.
[30] Brandenberg SJ, Zhao M, Boulanger RW, Wilson DW. p-y plasticity model for nonlinear dynamic analysis of piles in liquefiable soil. J Geotech Geoenviron Eng 2013;139(8):1262–74. https://doi.org/10.1061/(ASCE)GT.1943-5606.0000847.
[31] Kramer SL, Arduino P, Shin H. Using OpenSees for Performance-Based Evaluation of Bridges on Liquefiable Soils. Berkeley, CA: Pacific Earthquake Engineering Research Center; 2008.
[32] Taboada-Urtuzuastegui VM, Martinez-Ramirez G, Abdoun T. Centrifuge modeling of seismic behavior of a slope in liquefiable soil. Soil Dyn Earthq Eng 2002;22(9–12):1043–9. https://doi.org/10.1016/S0267-7261(02)00129-X.
[33] Das B. Principles of foundation engineering. 7th ed. Stamford, CT: Cengage Learning; 2011.
[34] Andersen KH, Schjetne K. Database of friction angles of sand and consolidation characteristics of sand, silt, and clay. J Geotech Geoenviron Eng 2013;139(7):1140–55. https://doi.org/10.1061/(ASCE)GT.1943-5606.0000839.
[35] Mazzoni S, McKenna S, Scott MH, Fenves GL. Open System for Earthquake Engineering Simulation. Berkeley, CA: Pacific Earthquake Engineering Research Center; 2007.
[36] Andrus RD, Stokoe KH, Andrus BRD, Stokoe KH. Liquefaction resistance of soils from shear-wave velocity. J Geotech Geoenviron Eng 2000;126(11):1015–25. https://doi.org/10.1061/(ASCE)1090-0241(2000) 126:11(1015).
[37] Hardin BO, Drnevich VP. Shear modulus and damping in soils: measurement and parameter effects. J Soil Mech Found Div 1972;98(6):603–24. https://doi.org/10.1016/0022-4898(73)90212-7.
[38] Wang X. Seismic failure mechanism and post-earthquake damage assessment method for pile-supported bridges in liquefied ground [Ph.D. thesis]. Tongji University; 2018.
[39] Hutchinson TC, Chai YH, Boulanger RW, Idriss IM. Inelastic seismic response of extended pile-shaft-supported bridge structures. Earthq Spectra 2004;20(4):1057–80. https://doi.org/10.1193/1.1811614.
[40] Khosravifar A, Boulanger RW, Kunnath SK. Effects of liquefaction on inelastic demands on extended pile shafts. Earthq Spectra 2014;30(4):1749–73. https://doi.org/10.1193/032412EQS105M.
[41] Wang X, Shafieezadeh A, Ye A. Optimal intensity measures for probabilistic seismic demand modeling of extended pile-shaft-supported bridges in liquefied and laterally spreading ground. Bull Earthq Eng 2018;16(1):229–57. https://doi.org/10.1007/s10518-017-0199-2.
[42] Wang X, Shafieezadeh A, Ye A. Optimal EDPs for post-earthquake damage assessment of extended pile-shaft-supported bridges subjected to transverse spreading. Earthq Spectra 2019;35(3):1367–96. https://doi.org/10.1193/090417EQS171M.
[43] Alipour A, Shafei B, Shinozuka M. Reliability-based calibration of load and resistance factors for design of RC bridges under multiple extreme events: scour and earthquake. J Bridg Eng 2012;18(5):362–71. https://doi.org/10.1061/(ASCE)BE.1943-5592.0000369.
[44] Mander JB, Priestley MJN, Park R. Theoretical stress-strain model for confined concrete. J Struct Eng 1988;114(8):1804–26. https://doi.org/10.1061/(ASCE)0733-9445(1988) 114:8(1804).
[45] Filippou FC, Popov EP, Bertero VV. Effects of bond deterioration on hysteretic behavior of reinforced concrete joints. Earthquake Engineering Research Center, Report No. EERC 83-19, University of California, Berkeley. 1983.
[46] Aviram A, Mackie K, Stojadinović B. Guidelines of nonlinear analysis of bridge structures in California. Berkeley, CA: Pacific Earthquake Engineering Research Center; 2008.
[47] Zhang J, Huo Y. Evaluating effectiveness and optimum design of isolation devices for highway bridges using the fragility function method. Eng Struct 2009;31(8):1648–60. https://doi.org/10.1016/j.engstruct.2009.02.017.
[48] AASHTO. AASHTO LRFD bridge design specifications. 6th ed. Washington, D.C.: American Association of State Highway and Transportation Officials (AASHTO); 2012.
[49] Dhakal RP, Su J. Design of transverse reinforcement to avoid premature buckling of main bars. Earthq Eng Struct Dyn 2018;47(1):147–68. https://doi.org/10.1002/eqe.2944.
[50] Brandenberg SJ, Kashighandi P, Zhang J, Huo Y, Zhao M. Fragility functions for bridges in liquefaction-induced lateral spreads. Earthq Spectra 2011;27(3):683–717. https://doi.org/10.1193/1.3610248.
[51] Pang Y, Wu X, Shen G, Yuan W. Seismic fragility analysis of cable-stayed bridges considering different sources of uncertainties. J Bridg Eng 2014;19(4):04013015. https://doi.org/10.1061/(ASCE)BE.1943-5592.0000565.
[52] Celarec D, Dolšek M. The impact of modelling uncertainties on the seismic performance assessment of reinforced concrete frame buildings. Eng Struct 2013;52:340–54. https://doi.org/10.1016/j.engstruct.2013.02.036.
[53] Barbato M, Gu Q, Conte JP. Probabilistic push-over analysis of structural and soil-structure systems. J Struct Eng 2010;136(11):1330–41. https://doi.org/10.1061/(ASCE)ST.1943-541X.0000231.
[54] Jones A, Kramer S, Arduino P. Estimation of uncertainty in geotechnical properties for performance-based earthquake engineering. Berkeley, CA: Pacific Earthquake Engineering Research Center; 2002.
[55] Mokwa RL. Investigation of the resistance of pile caps to lateral loading. Virginia Tech, 1999.
[56] Nielson BG, Desroches R. Seismic fragility methodology for highway bridges using a component level approach. Earthq Eng Struct Dyn 2007;36(11):823–39. https://doi.org/10.1002/eqe.
[57] Wang Z, Dueñas-Osorio L, Padgett JE. Influence of scour effects on the seismic response of reinforced concrete bridges. Eng Struct 2014;76:202–14. https://doi.org/10.1016/j.engstruct.2014.06.026.
[58] Wang Z, Dueñas-Osorio L, Padgett JE. Influence of soil-structure interaction and liquefaction on the isolation efficiency of a typical multispan continuous steel girder bridge. J Bridg Eng 2014;19(8):A4014001. https://doi.org/10.1061/(ASCE)BE.1943-5592.0000526.
[59] Baker JW, Lin T, Shahi SK, Jayaram N. New ground motion selection procedures and selected motions for the PEER transportation research program. Berkeley, CA: Pacific Earthquake Engineering Research Center; 2011.
[60] Gehl P, Douglas J, Seyedi DM. Influence of the number of dynamic analyses on the accuracy of structural response estimates. Earthq Spectra 2015;31(1):97–113. https://doi.org/10.1193/102912EQS320M.
[61] Arias A. A measure of earthquake intensity. Santiago, Cambridge, MA: MIT, Cambridge and University of Chile; 1970.
[62] Kayen RE, Mitchell JK. Assessment of liquefaction potential during earthquakes by Arias intensity. J Geotech Geoenviron Eng 1997;123(12):1162–74. https://doi.org/10.1061/(ASCE)1090-0241(1997) 123:12(1162).
[63] Dashti S, Karimi Z. Ground motion intensity measures to evaluate I: the liquefaction hazard in the vicinity of shallow-founded structures. Earthq Spectra 2017;33(1):241–76. https://doi.org/10.1193/103015EQS162M.
[64] Wang Z, Dueñas-Osorio L, Padgett JE. Optimal intensity measures for probabilistic seismic response analysis of bridges on liquefiable and non-liquefiable soils. Struct. Congr. 2012, Reston, VA: ASCE 2012. p. 527–38. https://doi.org/10.1061/9780784412367.047.
[65] Wang X, Ye A, Shafieezadeh A, Padgett JE. Fractional order optimal intensity measures for probabilistic seismic demand modeling of extended pile-shaft-supported bridges in liquefiable and laterally spreading ground. Soil Dyn Earthq Eng 2019;120:301–15. https://doi.org/10.1016/j.soildyn.2019.02.012.
[66] Shang Y, Ye A, Wang X. Shake table test of pile supported bridge under scour condition. China J Highw Transp 2017;30(12):280–9. (in Chinese).
[67] Li H, Liu S, Tong L, Xu X. Investigating the resonance compaction effect on laterally loaded piles in layered soil. Eng Geol 2018;246:1–11. https://doi.org/10.1016/j.enggeo.2018.09.019.